We are IntechOpen, the world's leading publisher of Open Access books Built by scientists, for scientists

4,800
Open access books available

122,000
International authors and editors

135M
Downloads

Our authors are among the

154
Countries delivered to

TOP 1%
most cited scientists

12.2%
Contributors from top 500 universities

CLARIVATE ANALYTICS BOOK CITATION INDEX INDEXED

WEB OF SCIENCE™

Selection of our books indexed in the Book Citation Index in Web of Science™ Core Collection (BKCI)

Interested in publishing with us?
Contact book.department@intechopen.com

Numbers displayed above are based on latest data collected.
For more information visit www.intechopen.com

4

Relativistic Density – Functional Study of Nuclear Fuels

Masayoshi Kurihara and Jun Onoe
Research Laboratory for Nuclear Reactors and Department of Nuclear Engineering, Tokyo Institute of Technology, Tokyo Japan

1. Introduction

Among nuclear materials used in both research and commercial power reactors, very high-density dispersion fuels have been used for requirement of a large proportion of uranium per unit volume in order to compensate to the reduction of enrichment (Meyer et al., 2002, Kim et al., 1999, 2002). For examples, uranium (U) with 10 wt% molybdenum (Mo) dispersed in aluminum (Al) matrix (Meyer et al., 2002, Kim et al., 2002) and U_3Si_2/ Al dispersion fuel (Kim et al., 1999) have been hitherto examined. Furthermore, zirconium (Zr) based U/ plutonium (Pu) alloys have recently been focused as a promising fuel for advanced reactors (Chernock & Horton, 1994).

U metals have α (orthorhombic)-, β (tetragonal)-, and γ (body centered cubic)-phases that depend on the ambient temperature (Chiotti et al., 1981). The α- and β-U phases form solid solutions with other metal elements to a limited extent (Chiotti et al., 1981), whereas the γ-U phase forms solid solutions with other elements to any extent (Chiotti et al., 1981). In addition, the α-U phase forms many intermetallic compounds with other metal elements (Kaufman, 1961). In these reasons, some α- and/ or γ-U/ transition metal (TM) alloys have been used in research reactors (Chiotti et al., 1981, Kaufman, 1961). To use advanced nuclear fuels practically, it is critical to understand the dissolution process of TM atoms into γ-U on the basis of their phase diagrams.

The alloying behavior of U compounds has been hitherto theoretically investigated by considering the relative stabilities of electronic configurations (Buzzard, 1955, Park & Buzzard, 1957) and the thermodynamics (Ogawa et al., 1995). Hume-Rothery has focused on the metallic radius of TM elements as a parameter for understanding their alloying behavior (Hume-Rothery & Raynor, 1954). According to their empirical findings, when the difference in the metallic radius between solute and solvent atoms is less than 15%, TM elements are very soluble to each other. Figure 1 shows the correlation between U/ TM radius and the maximum solid solubility (MSS) of TM into γ-U. Here, the dashed line denotes the metal radius smaller by 15% than that of γ-U (Zachariasen, 1973, Pauling, 1960).

This rule seems to explain MSS for 3d-TM/ γ-U alloys, but cannot explain MSS for 4d- and 5d-TM/ γ-U alloys. Furthermore, Buzzard pointed out that the miscibility of TMs into γ-U

depends on compatibility factors considering ionic radius, electron negativity, and the number of d-electrons (Buzzard, 1955, Park & Buzzard, 1957). However, because many empirical parameters should be determined, this evaluation process of their alloying behaviors is not applicable to other actinide alloy systems. On the other hand, Ogawa et al. investigated the alloying behavior by using the ChemSage program, and concluded that the difference in the excess free energy (ΔG^E) of the U/ Mo, U/ rhodium (Rh), and U/ palladium (Pd) alloying systems may be due to the contribution of the U6d-Pd4d orbital interactions (Ogawa et al., 1995). Although the interactions indeed play an important role of their alloying behaviors, it is necessary to clarify what interactions between γ-U and TMs contribute to the alloying behavior quantitatively in order to satisfactorily understand the alloying behavior of the 3d, 4d and 5d TMs into γ-U solid.

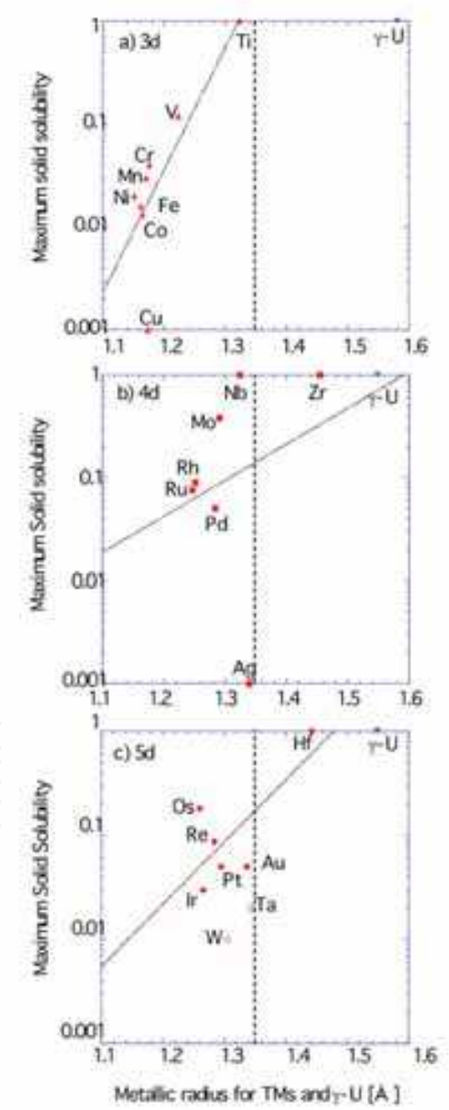

Fig. 1. The correlation between the metallic radius of TMs and the maximum solid solubility for γ-U alloyed with (a) 3d TMs, (b) 4d TMs, and (c) 5d TMs [Kurihara et al., (2008)]

Recently, some groups have theoretically studied the thermodynamic properties of U/ TM alloys. Landa et al. have examined the phase equilibrium of U/ Zr alloys, using the scalar-relativistic Green's function technique based on Korrings-Kohn-Robstoker (KKR) method (i.e. without spin-orbit coupling) (Landa et al., 2009). They obtained a good agreement between theoretical and experimental results for the ground-state properties of γ- (bcc) and δ- (C32) phases of U/ Zr alloys. On the other hand, Li et al. have obtained the thermodynamic assessments for thorium (Th)/ U and Th/ Zr binary and Th/ U/ Zr ternary alloys (Li et al., 2009), using the CALPHAD (calculation of phase diagrams) method based on experimental data including the phase equilibria and thermodynamic properties of the alloys. They have also obtained a good agreement between the calculated phase equilibria and experimental data. *Ab initio* calculations based on density-functional theory have also been used to examine the thermodynamic properties of U/ Al systems (Alonso et al., 2009, Sedmidudbsky et al., 2010). To understand the dissolution of elements into solid U in addition to obtain the phase diagram or phase equilibria, it is indespensable to determine which electronic terms contribute to the thermodynamic properties of U alloys by comparing density-functional calculations with experimental results.

We have previously investigated the alloying behavior of 3d-, 4d- and 5d-TMs into γ-U, using the discrete-variational Dirac-Fock-Slater molecular orbital (MO) method (R-DFT) which takes into account fully relativistic effects including the spin-orbit coupling (Kurihara et al., 2004, 2008, 2011). We have found that the maximum solid solubility (MSS) of TMs into γ-U is exponentially proportional to both the d-orbital energy of TM (Md) and the orbital overlap population (OOP) between TMd and U6d atomic orbitals.

In this chapter, we firstly introduce the relativistic discrete-variational Xα molecular orbital method (R-DFT) (Rosen et al., 1975, Adachi et al., 1977, Nakamatsu et al., 1991), secondary introduce our recent works on analysis of the valence photoelectron spectra of uranium carbides (UC) and α-U metal, and thirdly show the elucidation of the alloying behavior of TMs into γ-U metal using the R-DFT, and finally summarize the results obtained using R-DFT and describe the perspective for the quantum design of nuclear fuels for advanced reactors.

2. Computational method

2.1 Relativistic density-functional method

The present R-DFT method has been shown to be a powerful tool for the study of the electronic structures of molecules containing heavy elements such as uranium (Onoe et al., 1992a, 1994b, Hirata et al., 1997a, Kurihara et al., 1999, 2000). The one-electron molecular Hamiltonian, H, in the R-DFT method is written as,

$$\boldsymbol{H} = c\boldsymbol{\alpha}\boldsymbol{P} + \boldsymbol{\beta}mc^2 + V(r)\,. \tag{1}$$

Here, c, $\boldsymbol{P}$, m, $\boldsymbol{\alpha}$, $\boldsymbol{\beta}$ and $V(r)$ respectively denote the velocity of light, the operator of momentum, the mass of electron, Dirac matrices and the sum of Coulomb and exchange potentials. The molecular orbitals (MOs) are obtained by taking a linear combination of atomic orbitals (AOs). Details of the R-DFT method have been described elsewhere (Rosen et al., 1975, Onoe et al., 1993).

Basis functions, which are numerical solutions of the atomic Dirac-Fock-Slater equations for an atomic-like potential, are obtained at the initial stage of individual iterations of self-

consistent procedures (Adachi et al., 1977). The atomic-like potentials used to generate the basis functions are derived from the spherical average of the molecular charge density around nuclei. One-center (atomic) charges are estimated using Mulliken population analysis (Mulliken et al., 1955a, 1955b, 1955c, 1995d) for application to the self-consistent charge (SCC) method (Rosen et al., 1976) that is used to approximate the self-consistent field.

Morinaga et al have first found that the d-electron energy (Md) plays an important role for the alloying behavior (Morinaga et al., 1984, 1985a, 1985b, 1985c, 1991, 2005). In a similar manner, we have evaluated the Md of TMs in γ-U/ TM alloys from a weighted average of each component ($d_{3/2}$ and $d_{5/2}$), along with the U6d orbital energy. To compare Md values obtained for all TMs and U with each other, Md was shifted with respect to the Fermi level (E_F) of γ-U used as a reference (Morinaga et al., 1984, 1985a).

Since the orbital overlap population (OOP) expresses the strength of covalent interactions between AOs, it is a powerful tool to clarify the contribution of individual AOs to covalent bonding (Onoe et al., 1997c). In order to obtain information of the covalent bonding, we employed the Mulliken population analysis (Mulliken et al., 1955a, 1955b, 1955c, 1995d). In the present analysis, the number of electrons (n_i) was partitioned into the gross of the ith AO,

$$n_i = \sum_{(l,j)} \phi_l C_{il} C_{jl} S_{ij}, \tag{2}$$

Here, ϕ_l is the occupancy of the lth MO, $C_{il}(C_{jl})$ is the coefficient of the linear combination of AOs, and S_{ij} is the overlap integral between the ith and jth AOs. Two-center charges were estimated from the overlap populations (ith AO of γ-U and jth AO of TM),

$$n_{ij} = \sum_{(l)} \phi_l C_{ij} C_{jl} S_{ij}. \tag{3}$$

The effective charges for γ-U/ TM alloys were evaluated, because they are strongly related to the charge transfer (CT) between TM and γ-U.

2.2 Cluster model

Unlike band structure calculations of condensed matters obtained using their unit cells with a periodic boundary condition, the present R-DFT method employed a cluster model reflecting the crystal structure.

2.2.1 Uranium carbide

For a cluster model of uranium carbides (UC) with a NaCl-type structure, we made neutral UC_6, CU_6, and CU_6C_{18} cluster models with Oh symmetry and with a U-C bond length of 248.1 pm taken from the experimental results (Erode, P., 1983), as shown in Fig. 2.

In case of the CU_6C_{18} cluster, the CU_6 cluster was embedded with eighteen carbon atoms. Since the spin function is included in the Dirac equation explicitly, the Oh symmetry reduces to the Oh* double group (Bethe, H., 1929). Symmetry orbitals for the irreducible representations of Oh* symmetry were constructed from AOs by the projection operator method (Meyer, J. et al., 1989). All the calculations were performed with the Slater exchange parameter α of 0.7. The DV sample points of 6000 were used for the UC_6 and CU_6 models,

while 16,000 points for the CU_6C_{18} model. The basis functions up to the 7p orbital were used for U atom and those up to the 2p orbital were used for C atom. All the calculations were carried out self-consistently until the difference between the initial and final orbital populations in the iteration was less than 0.01.

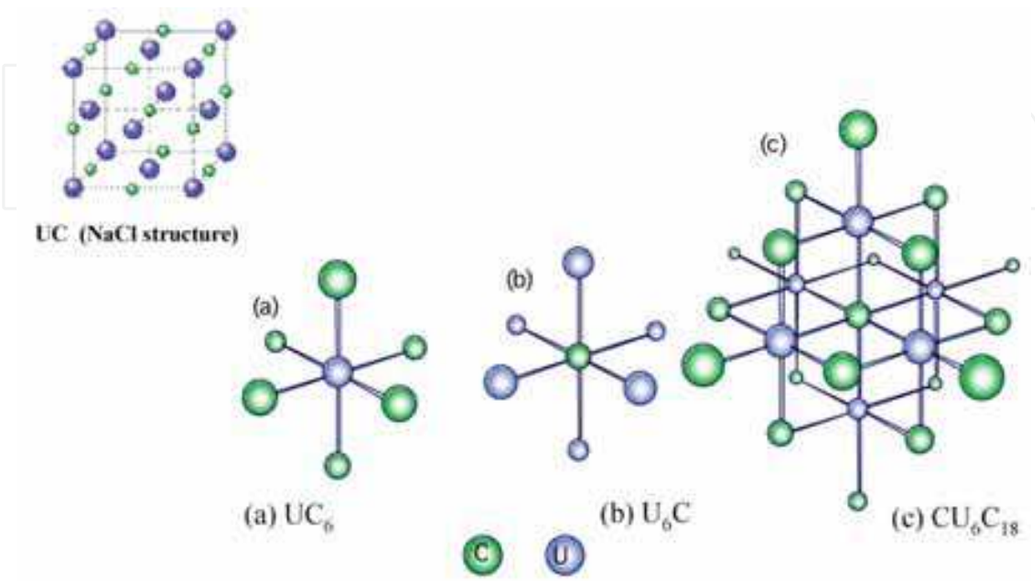

Fig. 2. Schematic illustration of cluster models for UC with a NaCl-type crystal structure: (a) UC_6, (b) CU_6, and (c) CU_6C_{18} [Kurihara et al., (1999)]

2.2.2 α-Uranium metal

Figure 3 shows (a) the unit cell of α-U metal crystal with an orthorhombic structure and (b) the U_9 cluster model with the central U atom (1) surrounded by eight U atoms (2)-(8).

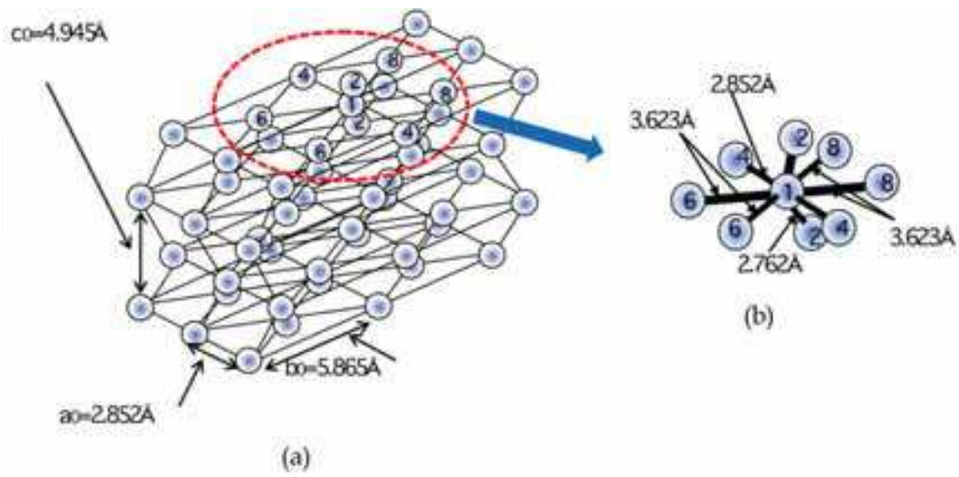

Fig. 3. Schematic illustration of α-U metal: (a) the orthorhombic structure of α-U metal and (b) a U_9 cluster model used as the minimum unit of α-U crystal structure [Kurihara et al., (2000)].

The geometry of the present cluster has a C_{2v} symmetry with the U-U bond length of 5.219 au for (1)-(2), 5.389 au for (1)-(4), and 6.165 au for (1)-(6) and (1)-(8) on the basis of the experimental results of α-U metal (Holden, A. N., 1958). Here, "au" denotes the atomic unit (1 au = Bohr radius). Symmetry orbitals for the irreducible representations of C_{2V}^* symmetry were constructed from AOs by the projection operator method. All the calculations were performed with the Slater exchange parameter α of 0.7. The DV sample points of 18,000 were used for the U_9 cluster model. The basis functions up to the 7p orbital were used for U atom. All the calculations were carried out under the same conditions as for UC.

2.2.3 γ-Uranium/transition metal alloy

Figure 4 shows schematic representation of a cluster model of γ-U alloyed with TMs. As shown in Fig. 4, the central U atom, U(1), was substituted with TM atoms. To compare the difference in the electronic structure among the γ-U/ TM alloys, the MO energy level structure and chemical bonding of the alloys were examined (Kurihara et al., 2004). In the present works, the lattice relaxation in association with TM element substitution to γ-U solid was ignored, because the Md and OOP may not be affected significantly by the lattice relaxation (Morinaga et al., 1984, 1985a, 1985b). The lattice constant of γ-U crystal was taken from the experimental result of 6.659 au (Holden 1958).

Symmetry orbitals for the irreducible representations of D_{4h}^* symmetry were constructed from the AOs by the projection operator method. The present R-DFT calculations were performed with the Slater exchange parameter α of 0.7 and with 18,000 DV sample points for the U_8-TM cluster model. The basis functions were used to be the 1s-7p AOs for U atom, the 1s-4p AOs for 3d TMs, the 1s-5s AOs for 4d TMs, and the 1s-6s AOs for 5d TMs. All the calculations were carried out self-consistently under the same conditions as for UC and α-U.

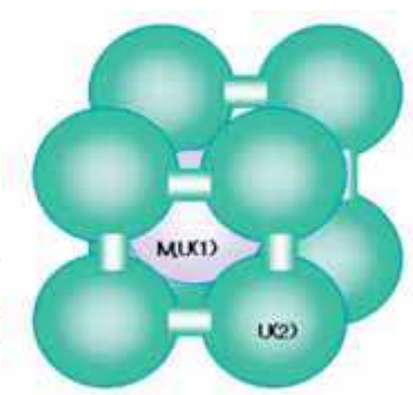

Fig. 4. Schematic illustration of TM/ γ-U alloy cluster model: the central U atom (1) replaced with TM atom [Kurihara et al., (2004)]

2.3 Theoretical x-ray photoelectron spectra

XPS (X-ray photoelectron spectroscopy) intensity was estimated using the following equation (Gellius, U., 1974),

$$I_l = \sum_i \sigma_i P_{il} \,. \tag{4}$$

Here, I_l is the probability of photo-ionization from the lth MO level, σ_i is the photo-ionization cross-section of the ith atomic orbital, and P_{il} is the population of the ith atomic orbital in the lth MO. The photo-ionization cross-section of individual AOs was taken from the data estimated by *ab initio* calculations (Scofield, J. H., 1976). The cross-section of the U7p was ignored in the present calculations, because it was too small to contribute to the XPS intensity. For evaluating P_{il}, the gross population of individual AOs for each MO was evaluated by Mulliken population analysis (Mulliken et al., 1955a, 1955b, 1955c, 1995d). Theoretical XPS spectra were obtained by replacing each stick peak with a Lorentzian curve with a full width at the half maximum (FWHM) of 1.46 eV. We then compared these with the experimental XPS spectra of UC solid (Ejima, T., et al., 1993).

In a similar manner to that for UC solid, theoretical XPS spectra of α-U solid were obtained by replacing each stick peak with that with a FWHM of 1.6 eV. Then, we compared these with the experimental XPS for α-U metal (Fuggle, J. C., et al., 1982).

3. Relativistic effects in molecules

In this section, we briefly explain relativistic effects on the electronic structure and chemical binding in molecules for understanding the results of uranium compounds introduced in Sections 4 and 5. Prior to describing the effects in molecules, we begin to explain the relativistic effects in atoms. The Bohr radius (a) and the energy (E) of hydrogen-like atoms are respectively given by the following equations,

$$a = \frac{n^2\hbar^2}{mZe^2}, \tag{5}$$

and

$$E = -\frac{me^2Z^2}{2\hbar^2n^2}. \tag{6}$$

Here, m is the mass of electron, n is the principal quantum number, Z is the atomic number, e is the elementary charge, $\hbar$ is Planck's constant. In addition, the ratio of the speed of 1s electron (v_{1s}) to that of light (c) can be written by Z/ 137. For U atom with Z=92, the v_{1s} can be estimated to be 0.67c, which indicates that the relativistic effects should be considered in quantum formula. Even for the U6s valence atomic orbital, the v_{6s} is calculated to be 0.1c, implying that the relativistic effects can appear in the valence region that is related to chemical bonding. According to the theory of relativity, the mass of electron is influenced by the relativistic effects, which can be given by the following equation,

$$m = \frac{m_0}{\sqrt{1-\left(\frac{v}{c}\right)^2}}. \tag{7}$$

Here, m_0 and v are the rest mass and speed of electron, respectively. Accordingly, one can see from Eqs. (5) and (6) that when m increases with increasing Z, Bohr radius and energy become contracted and increased, respectively. A heavier element exhibits more remarkable change in both a and E by the relativistic effects.

The relativistic effects on AOs can be classified into two categories: direct and indirect effects. The former effects result in the relativistic contraction of inner-shell orbitals (e.g. s and p orbitals). In addition, since the total angular momentum j (= l + s) is the quantum number in Dirac's equation, the energy splitting due to the spin-orbit interactions is simultaneously taken into account (e.g. 6p splits to $6p_{3/2}$ and $6p_{1/2}$) in the equation. On the other hand, the indirect effects cause the expansion of outer AOs (e.g. d and f AOs) due to the screening of nuclear charges by the contraction of the inner-shell AOs. As described above, these relativistic effects become magnified with increasing Z, and remarkably affect both valence electronic structure and chemical bonding of condensed matters (molecules, complexes, and solids) containing heavy elements such as uranium. We next explain how the relativistic effects affect the valence electronic structure and chemical bonding of UF_6 as an example.

3.1 Relativistic effects on valence electronic structures

Figure 5 shows the comparison between non-relativistic and relativistic one-electron energies of valence MOs for the ground state of UF_6 that is often used as a material for uranium enrichment. Here, MOs were classified into two parts based on inversion symmetry: "gerade" and "ungerade" shown on the left and right sides, respectively.

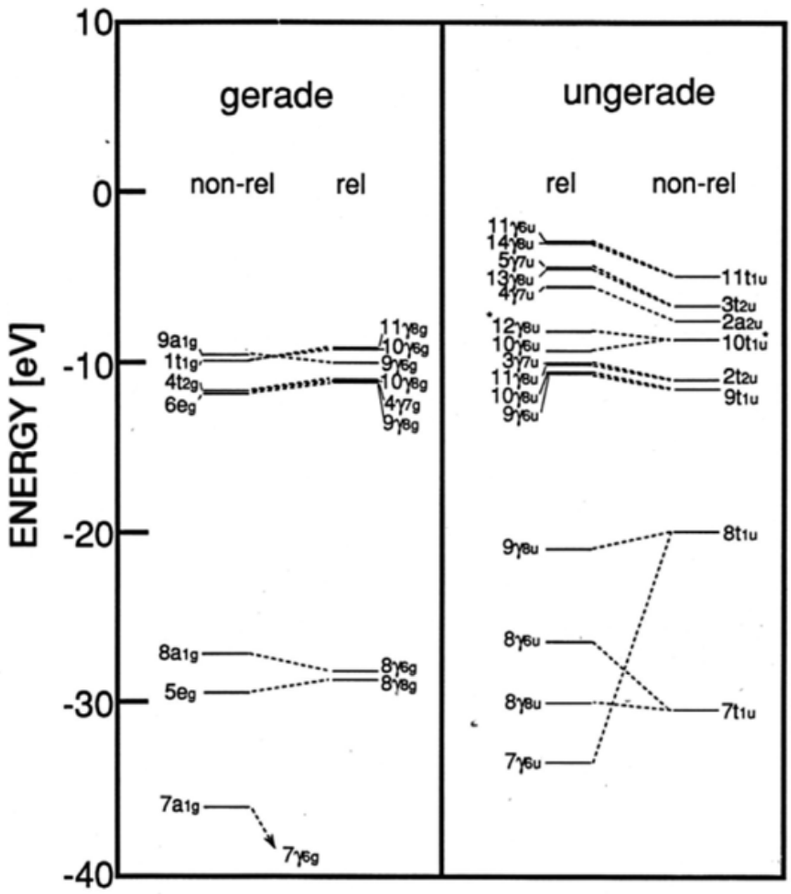

Fig. 5. Non-relativistic and relativistic one-electron energies for the ground state of UF_6 [Onoe et al., (1993)]

As shown in Fig. 5, two kinds of relativistic effects appear in the valence electronic structure: the energy splitting for several MOs and the upward or downward shift in the one-electron energy for individual MOs. In particular, since the energy splitting (ΔE) between the $U6p_{1/2}$ and $U6p_{3/2}$ (ΔE = 8.9 eV) is larger than that for both U5f (ΔE = 0.8 eV) and U6d (ΔE = 0.5 eV) AOs, the non-relativistic $7t_{1u}$ and $8t_{1u}$ MOs caused by the U6p-F2s interactions exhibit the noticeable splitting to form the four corresponding relativistic MOs. Indeed, we succeeded in assigning these four relativistic MOs in the valence photoelectron spectra of UF_6 (Onoe et al., 1994b).

3.2 Relativistic effects on chemical bonding

To understand how the relativistic effects influence the chemical bonding of UF_6, we have investigated the contribution of individual AOs to the chemical bonding by examining the non-relativistic and relativistic radial wave functions [Onoe et al., 1993]. Figure 6 shows the radial wave functions of the uranium valence atomic orbitals (5f, 6s, 6p, 6d) obtained using non-relativistic and relativistic density-functional calculations. For the relativistic radial wave functions, the small components were omitted and only the large ones were shown in Fig. 6, because the former ones play a minor role of contributing to chemical bonding. Figure 6 suggests that the relativistic contraction and expansion of the valence AOs at the U-F bond length significantly affect the strength of chemical bonding of UF_6.

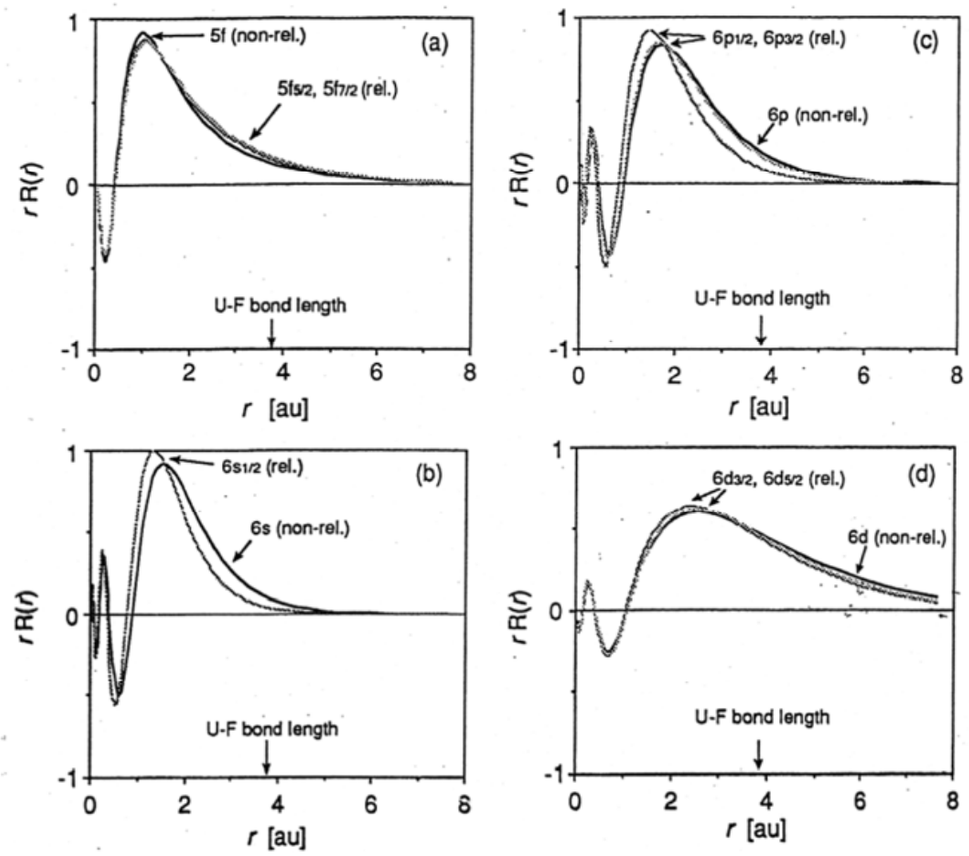

Fig. 6. Non-relativistic and relativistic radial wave functions [$R(r)$] of U valence atomic orbitals: (a) U5*f*, (b) U6*s*, (c) U6*p*, and U6*d* [Onoe et al., (1993)]

Since the orbital overlap population (OOP) is a good indicator for the strength of chemical bonding between AOs, we examined the OOP between individual U and F valence AOs, along with the bond overlap population (Bo) between U and F atoms, in order to clarify the contribution of the relativistic contracted and expanded AOs to the chemical bonding of UF_6.

Table 1 summarizes the OOP and Bo obtained from Mulliken population analysis for the non-relativistic and relativistic calculations. Here, the positive and negative signs of OOP imply the bonding and anti-bonding interactions, respectively. For an example, the strength of anti-bonding U6s-F2s and U6s-F2p interactions becomes weakened from non-relativistic to relativistic calculations, because the relativistic contraction of the U6s radial wave function reduces the U6s-F2s and U6s-F2p OOPs in the U-F bond region, as shown in Fig. 6. This results in the strengthening of the U-F bond. On the other hand, the relativistic expansion of the U5f and U6d radial wave function in the U-F bond region strengthens the U5f-F2p and U6d-F2p bonding interactions. The relativistic changes in the U valence AOs cause a large difference in the U-F chemical bond, as indicated in Table 1.

		DV-HFS (nonrelativistic) F		DV-DS (relativistic) F	
		2*s*	2*p*	2*s*	2*p*
U	5*f*	0.07	1.07	0.08	1.17
	6*s*	−0.16	−0.54	−0.05	−0.29
	6*p*	−0.56	−0.71	−0.42	−0.85
	6*d*	0.18	1.54	0.16	1.77
Total U–F bond overlap population		+1.21		+2.15	

Table 1. The overlap populations between U and F valence AOs for non-relativistic and relativistic calculations, along with the U-F bond overlap population [Onoe et al., (1993)]

4. Application to assign the valence X-ray photoelectron spectra of uranium metal and compounds

4.1 Uranium carbides

Figure 7 shows the experimental valence XPS spectra of UC (Ejima, et al., 1993) (a) and theoretical spectra for the UC_6 (b), CU_6 (c), and CU_6C_{18} (d) cluster models shown in Fig. 2, along with the partial density-of-states (pDOS) of the U5f and U6d AOs (e) and of the C2s and C2p AOs (f). As shown in Fig. 7(a), UC has the intense peak "1" at the Fermi level (E_F), the shoulder peak "2" at around -2 eV, and the broad weak peak "3" at around -10 eV. We next compared theoretical spectra [Fig. 7(b)-(d)] with the experimental result. As shown in Fig. 7(b), the UC_6 cluster model well reproduced both relative intensity and position (binding energy) for the peaks "1" and "3", but the shoulder peak "2" unfortunately seemed to be reproduced. On the other hand, the CU_6 cluster model showed a peak corresponding to the peak "2" besides the peaks "1" and "3", but it was completely separated (not a shoulder peak) from the peak "1". Accordingly, it is found that the CU_6 cluster model reproduces the experimental spectra better than the UC_6 cluster model. When the CU_6

cluster is surrounded with eighteen C atoms, a CU_6C_{18} embedded cluster model is expected to reproduce the experimental spectra better than the CU_6 cluster. Comparison between Figs. 7(a) and 7(d) indicates that the theoretical spectra well reproduce the whole experimental one.

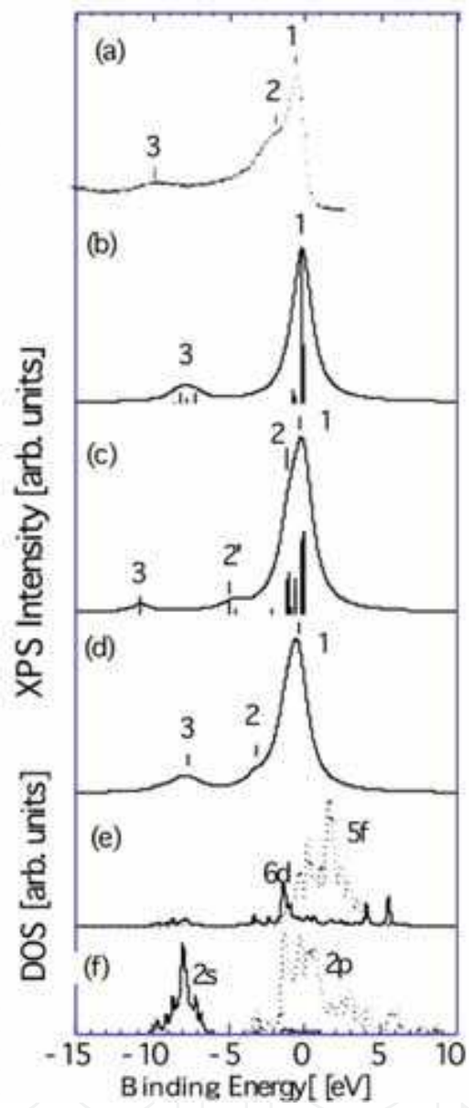

Fig. 7. Theoretical and experimental valence x-ray photoelectron spectra for UC: (a) experiment [Ejima. T., et al., (1993)] and theoretical spectra obtained using (b) UC_6, (c) CU_6, and (d) CU_6C_{18} cluster models, along with partial density-of-states (pDOS) for (e) the U5f (dashed line) and U6d (solid line) AOs and (f) the C2s (solid line) and C2p (dashed line) AOs [Kurihara et al.,(1999)]

To assign the three peaks shown in Fig. 7(a), we next examined the pDOS based on the results of the CU_6C_{18} embedded cluster model. Figures 7(e) shows the pDOS of the U5f (dashed line) and U6d (solid line) AOs, whereas Figure 7(f) shows that of the C2s (solid line) and C2p (dashed line) AOs. Comparison between Figs. 7(a) and 7(e, f) indicates that the intense peak "1" is mainly attributed to the U5f AO which has a large photo-ionization

cross-section and the shoulder peak "2" is attributed to the U6d-C2p AOs, whereas the broad weak peak "3" is mainly attributed to the C2s AO.

In previous reports by the other groups, Schalder et al reported that the intense peak "1" was due to the U5f-U6d bands, while the shoulder "2" due to the U6d-C2p band (Schadler, G. H., 1990). On the other hand, Ejima et al concluded that a small amount of the U5d component contributes to the shoulder "2". However, because the $U5d_{5/2}$ and $U5d_{3/2}$ AOs are respectively located at -91 eV and -99 eV, the U5d components can be considered to play a minor role for the shoulder "2". In fact, the present calculations show that the U5d components have no contribution to the valence electronic structure of UC.

4.2 α-Uranium metal

Figure 8 shows (a) the experimental (Fuggle, J. C., et al., 1974) and theoretical x-ray photoelectron spectra obtained using the U_9 cluster model (Kurihara, M., et al., 2000) for α-U metal, (b) the pDOS of U valence AOs, and (c) the magnified pDOS in the vicinity of E_F. As shown in Fig. 8(a), it is interesting to note that the theoretical spectra well reproduced the experimental one of α-U metal, in spite of using the minimum U_9 cluster model shown in Fig. 8. By comparison between Figs. 8(a) and 8(b), it is clearly found that the peaks "B" and "C" are only attributed to the $U6p_{3/2}$ and $U6p_{1/2}$ AOs, respectively. In a similar manner, the

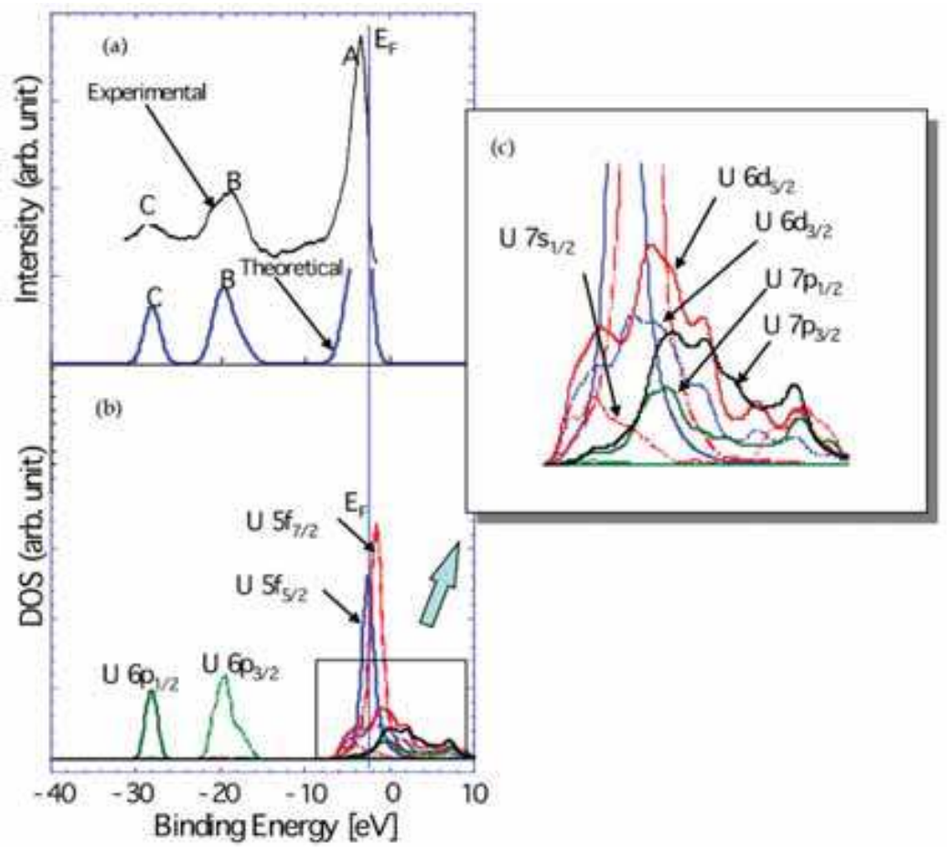

Fig. 8. (a) Experimental [Fuggle, et al., (1974)] and theoretical spectra, (b) partial density-of-states (pDOS) of U valence AOs and (c) magnified pDOS in the vicinity of E_F [Kurihara et al., (2000)]

intense peak "A" appearing at E_F is mainly attributed to the U5f$_{7/2}$ and U5f$_{5/2}$ AOs. As shown in Fig. 8(c), since the other valence AOs such as the U6d, U7s, and U7p are located around E_F, they contribute to the peak "A" to some extent. However, because their photo-ionization cross-sections are much smaller than that of the U5f AOs, they are considered to have minor contributions.

In previous band calculations (Yamagami. H., & Hasegawa. A., 1990), they compared the DOS structures with the experimental spectra, and discussed the assignment of each peak qualitatively. On the contrary, the present method can calculate XPS intensity of individual MOs for the cluster model used as the minimum unit of α-U metal. Thus we have quantitatively obtained the valence XPS spectra, together with pDOS of individual AOs contained in each MOs. This enables us to assign individual peaks satisfactorily.

5. γ-Uranium/transition metal alloys

As introduced in the previous section, the present R-DFT method well reproduced the experimental photoelectron spectra of UC and α-U solid and assigned the origins of individual peaks. In this section, we applied this method to understand what electronic factors play significant roles of the alloying behavior for γ-U/ TM metal alloys that are one of the candidates as nuclear fuels for advanced reactors.

5.1 Correlation between the Md (or effective charges) and the maximum solid solubility

The Md has been found to play an important role of alloying for Ni_3Al (Morinaga et al., 1984) and bcc Fe ((Morinaga et al., 1985a). In this section, we first present the correlation between the maximum solid solubility (MSS) and Md for γ-U/ TM alloys (Kurihara et al., 2004, 2008).

Figure 9 shows the plot of MSS as a function of Md, where the regression lines were obtained using a least square method. It is found that MSS is exponentially dependent on Md except for γ-U/ Ta and γ-U/ W alloys, though the reason of this exception is not still clearly understood. This exponential dependence will be discussed from a thermodynamic standpoint in Section 5.4.

Since Md is related to the charge transfer (CT) between the TM and γ-U, we next examined the correlation between MSS and CT (Kurihara et al., 2008). Figure 10 shows the plot of Md as a function of atomic number (Z) for individual TMs in γ-U/ TM alloys, along with the U6d energy of U(1) prior to TM substitution. The sign and amount of the difference between Md and U6d energies determine the direction and amount of CT between TM and γ-U, respectively. The CT takes place from TMs to γ-U when Md level is higher than the U6d one, whereas CT from γ-U to TMs takes place when Md level is lower than the U6d one. In addition, a larger difference between Md and U6d energies results in a larger amount of CT between them. From the results of Figs. 9 and 10, a smaller difference between the Md and U6d levels results in a larger MSS, as previously reported by Morinaga et al. (Morinaga et al., 1984, 1985a,b). Namely, a smaller amount of CT between TM and γ-U provides a larger MSS for γ-U/ TM alloys.

Since the amount of CT is directly related to the effective charge, we next examined the correlation between MSS and the effective charges on TM and U atoms (Kurihara et al.,

2008). Figure 11 shows that MSS exhibits a negatively exponential relationship with respect to the effective charge. This implies that MSS exhibits a negatively exponential dependence on the amount of CT between the TM and U atoms. Furthermore, because the effective charge indicates the degree of ionic bonding interaction between TMs and γ-U, it can be said that MSS shows a negatively exponential dependence on the strength of ionic bonding between TM and γ-U atoms. This indicates that a large ionic bonding between TM and γ-U atoms results in a smaller MSS for γ-U/ TM alloys.

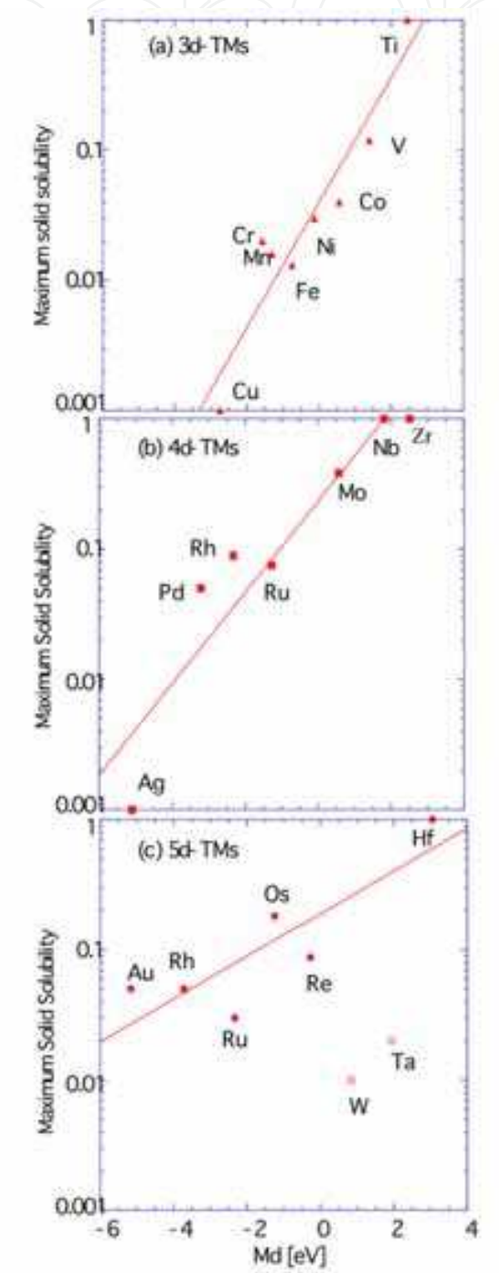

Fig. 9. Plot of the maximum solid solubility (MSS) as a function of Md for γ-U/ TM alloys [Kurihara et al., (2008)]

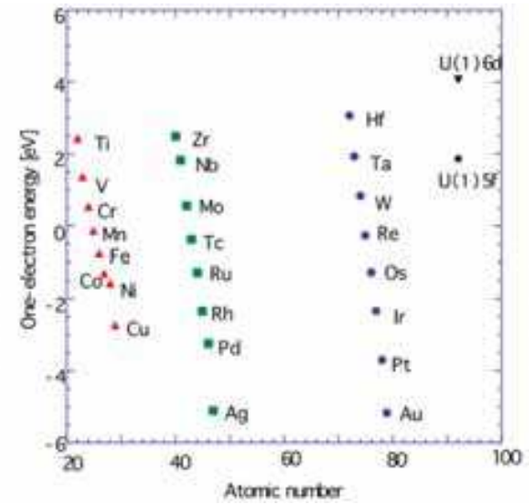

Fig. 10. Plot of Md as a function of atomic number (Z) for individual TMs in γ-U/ TM alloys, along with the U6d and U5f energies of U(1) prior to TM substitution [Kurihara et al., (2008)]

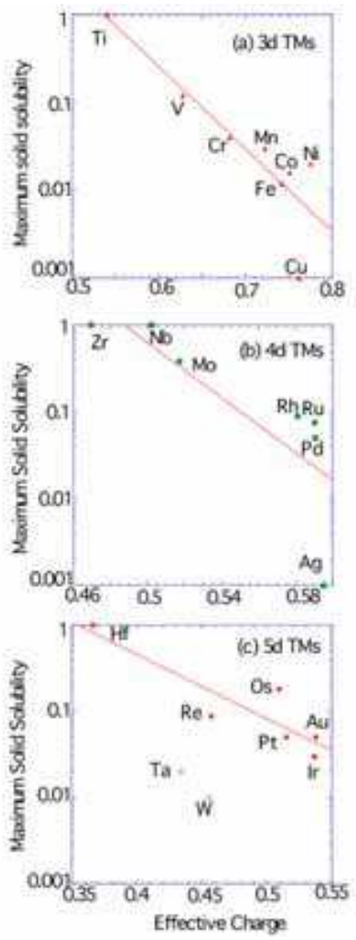

Fig. 11. The correlation between the maximum solid solubility (MSS) and the charge transfer (CT) between TM and U atoms for γ-U/ TM alloys [Kurihara et al., (2008)]

Since the bonding between TMs and γ-U contain not only ionic but also covalent interactions, we next discuss the correlation between MSS and the covalent interactions between TMs and γ-U.

5.2 Correlation between orbital overlap populations and the maximum solid solubility

We examined the correlation between TMd-U6d OOP and MSS for γ-U/ TM alloys, because OOP is a good indicator for the strength of the covalent bonding between TM and U atoms. Figure 12 shows the plot of MSS as a function of OOP between TMd and U6d AOs

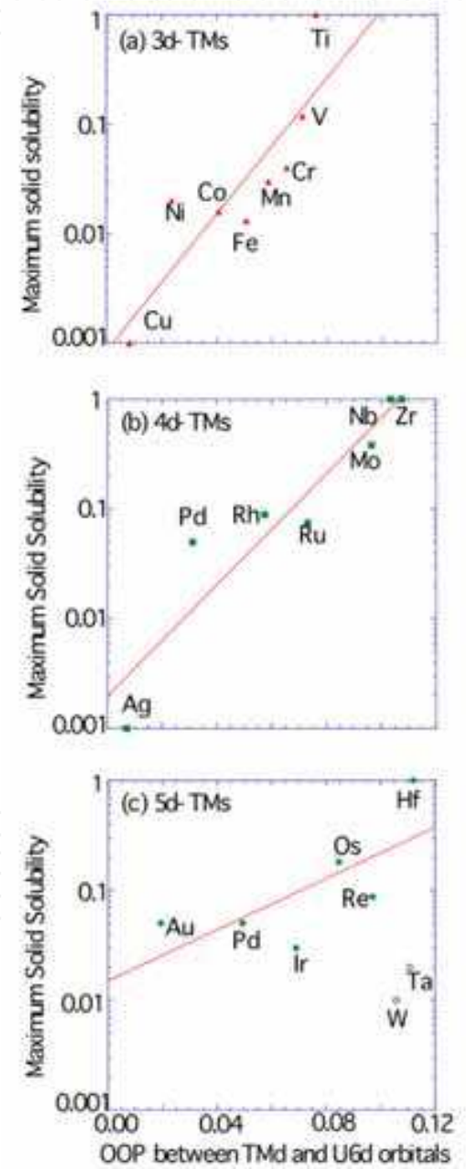

Fig. 12. The correlation between the maximum solid solubility (MSS) and the orbital overlap population (OOP) between TMd and U6d atomic orbitals: (a) 3d TMs, (b) 4d TMs and (c) 5d TMs [Kurihara et al., (2008)]

(Kurihara et al., 2008), and demonstrates that MSS exhibits an exponential dependence on the strength of the U6d-TMd covalent bonding. Namely, a stronger covalent bonding between TM and U atoms provides a larger MSS for TMs alloyed into γ-U. This is opposite to the correlation between MSS and the TM-U ionic bonding.

We will discuss the reason why MSS is exponentially proportional to OOP as well as Md in Section 5.4.

5.3 Role of U6d-TMd orbital interactions in alloying of γ-U/TMs

Figure 13 shows the plot of MSS as a function of the energy difference ($\alpha_U - \alpha_{TM}$) between the U6d and TMd AOs (Kurihara et al., 2011). The energy difference ($\alpha_U - \alpha_{TM}$), which is often used to discuss the CT between U and TM atoms, shows that MSS exhibits an inversely exponential dependence on ($\alpha_U - \alpha_{TM}$), thus a smaller value of ($\alpha_U - \alpha_{TM}$) provides a larger MSS. Since the energy difference ($\alpha_U - \alpha_{TM}$) is related to the magnitude of the CT between TM and γ-U, Figure 13 implies that a smaller CT between them gives rise to a larger MSS for γ-U/ TM alloys.

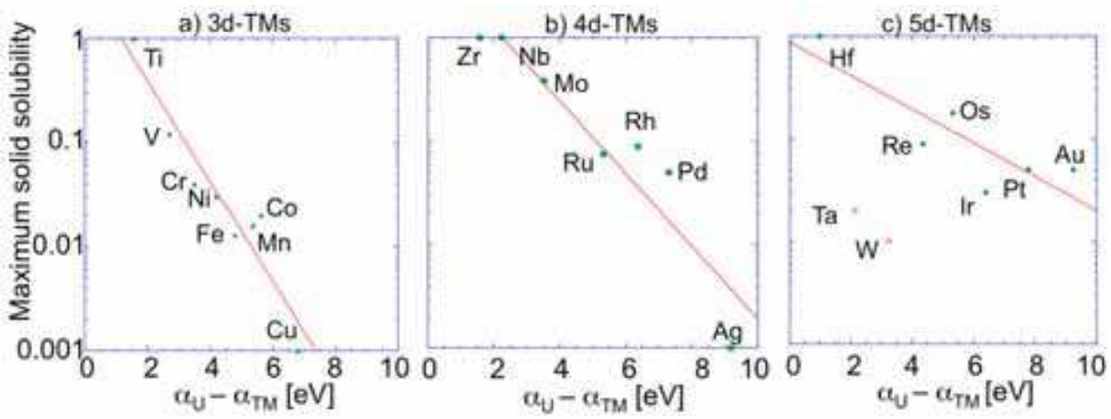

Fig. 13. Plot of the maximum solid solubility (MSS) as a function of the energy difference between the U6d (α_U) and TMd (α_{TM}) AOs [Kurihara et al., (2011)]

Figure 14 shows the correlation between the TMd-U6d OOP and MSS for γ-U/ TM alloys (Kurihara et al., 2011), and demonstrates the exponential dependence of MSS on the OOP for all γ-U/ TM alloys except for Ta and W elements. Thus, an increase in the OOP results in an increase in MSS of γ-U/ TM alloys.

From the results of Figs. 13 and 14, one can see that the interactions between TMd and U6d AOs play an important role of determining the magnitude of MSS for γ-U/ TM alloys. In other words, the TMd-U6d orbital interactions become a key parameter for estimating MSS of γ-U/ TM alloys. We next discuss the physical meaning of the TMd-U6d orbital interactions in the magnitude of MSS.

Figure 15 schematically illustrates the stabilization energy (ΔE) caused by the U6d-TMd orbital interactions from a viewpoint of molecular orbital theory (top) and the correlation between MSS and ΔE or the U6d-TMd energy difference (bottom). In the framework of the simple Hückel approximation (Hückel, E, 1931), ΔE is obtained as,

$$\Delta E = \frac{1}{2}\left[\sqrt{(\alpha_U - \alpha_{TM})^2 + 4\beta^2} - (\alpha_U - \alpha_{TM})\right]. \quad (8)$$

Here, α_U and α_{TM} respectively denote the U6d and TMd energies, and α_U is equal to or greater than α_{TM} ($\alpha_U \geq \alpha_{TM}$). β denotes the resonance integral between the TMd and U6d AOs, which can be written as,

$$\beta = \frac{1}{2}(\alpha_U + \alpha_{TM})KS$$

Where, K is a constant, and S is the overlap integral between the TMd and U6d AOs. Namely, β is proportional to S, thus proportional to the TMd-U6d OOP.

To discuss the correlation between ΔE and Md/ OOP more clearly, we introduce the following two variables, $t = (\alpha_U - \alpha_{TM}) \big/ 2|\beta|$ and $F(t) = \sqrt{t^2 - 1} - t$, into Eq. (8). Then, ΔE can be rewritten as,

$$\Delta E = F(t) \cdot |\beta|. \quad (9)$$

By considering the range of the two quantities on the right-hand side of Eq. (7) (i.e., $t \geqq 0$ and $0 < F(t) \leqq 1$), we obtained the range of the stabilization energy,

$$0 < \Delta E \leqq |\beta|. \quad (10)$$

Accordingly, ΔE is the maximum ($= |\beta|$) when $F(t)$ is unity at $t = 0$, that is, $\alpha_U = \alpha_{TM}$. On the contrary, ΔE becomes the minimum (near equal to zero) when ($\alpha_U - \alpha_{TM}$) is much larger than unity ($\gg 1$). Consequently, a larger MSS for γ-U/ TM alloys is obtained at a lower value of ($\alpha_U - \alpha_{TM}$) (corresponding to a larger ΔE), whereas a small MSS is obtained at a larger value of ($\alpha_U - \alpha_{TM}$) (corresponding to a smaller ΔE). Consequently, it can be concluded that the magnitude of ΔE caused by the TMd-U6d orbital interactions plays a key role of determining the magnitude of MSS.

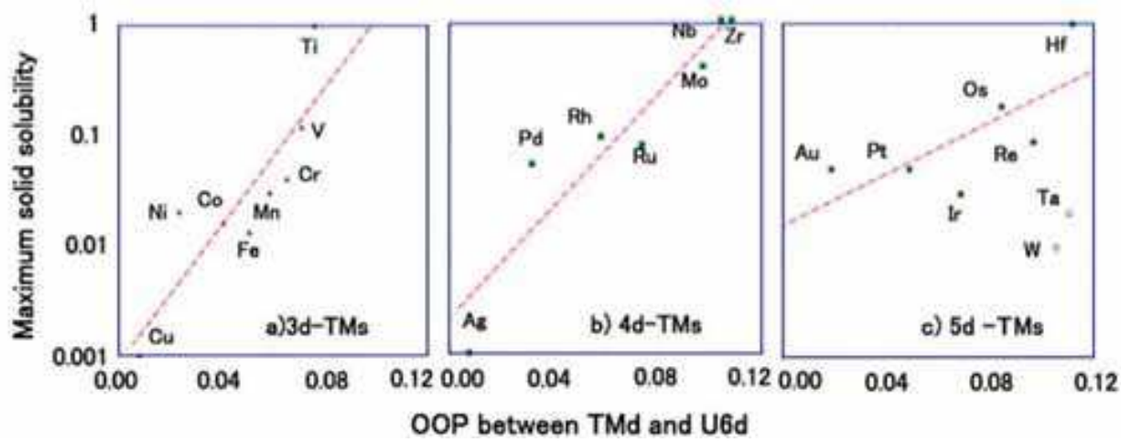

Fig. 14. Plot of the maximum solid solubility (MSS) as a function of OOP between the U6d and TMd AOs for γ-U/ TM alloys [Kurihara et al., (2011)]

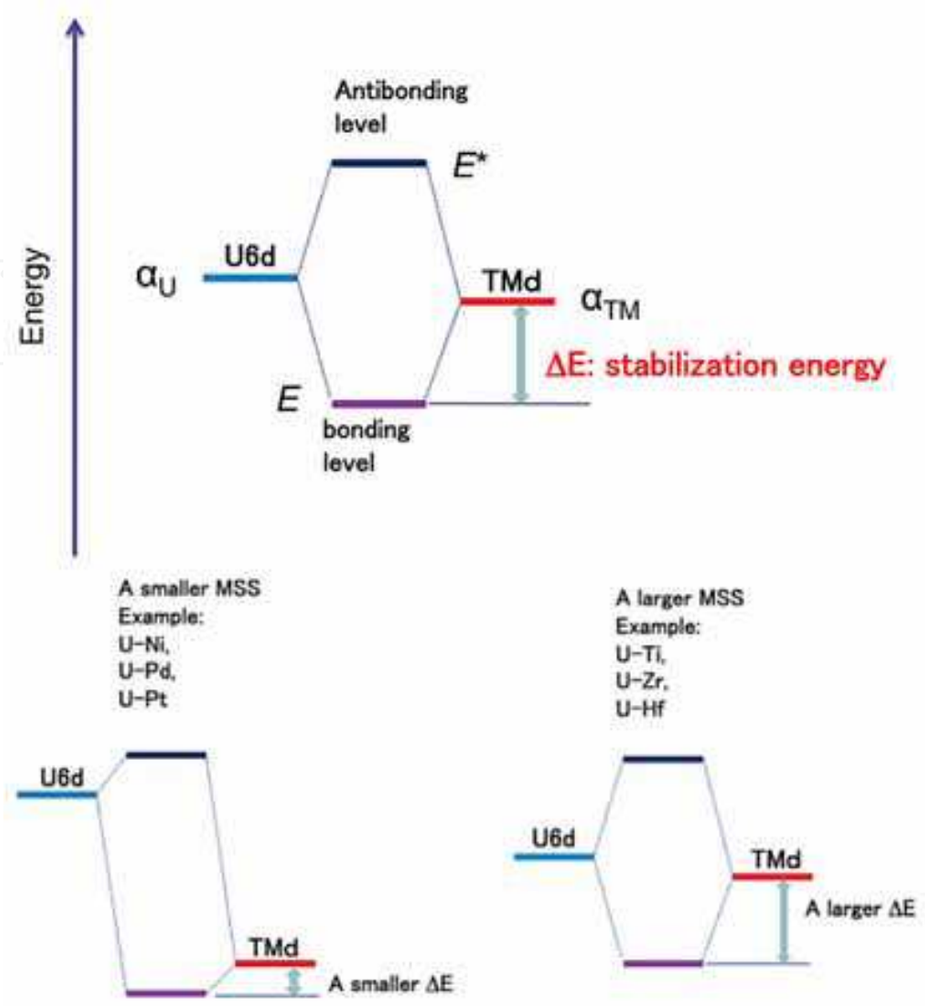

Fig. 15. Schematic illustration of the TMd-U6d orbital interactions based on molecular orbital theory (Top) and of the correlation between MSS and the stabilization energy (ΔE) caused by their orbital interactions (Bottom) [Kurihara et al., (2011)]

5.4 Exponential dependence of MSS on Md and OOP

As shown in Figs. 9 and 12, MSS exhibits an exponential dependence on both Md [in other words, the U6d-TMd energy difference (α_U - α_{TM})] and the U6d-TMd OOP. In the present work, we employed the cluster model (see Fig. 4) for γ-U/ TM alloys by substituting the central U atom with TM atoms. The following equilibrium has been considered based on the cluster model,

$$U_9 + TM \Leftrightarrow U_8TM + U\,. \tag{11}$$

Here, TM denotes a TM atom in the TM bulk phase, while U_9/ U_8TM and U respectively denote a cluster and a U atom in the γ-U bulk phase. As the equilibrium constant (K) in Eq. (11) increases, the concentration of U_8TM increases, thus increasing MSS. On the other hand, as K decreases, the U_8TM concentration correspondingly decreases, thus reducing MSS.

Accordingly, MSS is proportional to K. Then the relation between MSS and K can be written as,

$$MSS \propto K = Ae^{-\Delta G/RT}. \tag{12}$$

Where, A is a constant, ΔG denotes the difference in Gibbs free energy before and after the substitution, R is the gas constant, and T is the absolute temperature. Since the lattice relaxation associated with substitution of TM into γ-U solid was negligible in the present calculations, the entropy remained constant (ΔS = 0) before and after the TM substitution. Thus, ΔG is equal to the enthalpy difference (ΔH) before and after the substitution. Accordingly, Eq. (12) can be rewritten as,

$$MSS \propto K = Ae^{-\Delta G/RT} = Ae^{-\Delta H/RT}. \tag{13}$$

Since ΔH includes ΔE caused by the TMd-U6d orbital interactions, the following relationship is obtained,

$$MSS \propto K = Ae^{-\Delta G/RT} = Ae^{-\Delta H/RT} \propto e^{\Delta E/RT}. \tag{14}$$

Since ΔE is proportional to both ($\alpha_U - \alpha_{TM}$) and S, it can be understood that MSS depends exponentially on both Md and OOP, as shown in Figs. 9 and 12.

In the above discussion, Md and OOP can be regarded as a good parameter to determine the magnitude of MSS. Then we next made the OOP–Md map for γ-U/ TM alloys (Kurihara et al, 2011), as shown in Fig. 16. Interestingly, γ-U/ TM alloys with a smaller MSS appear in a

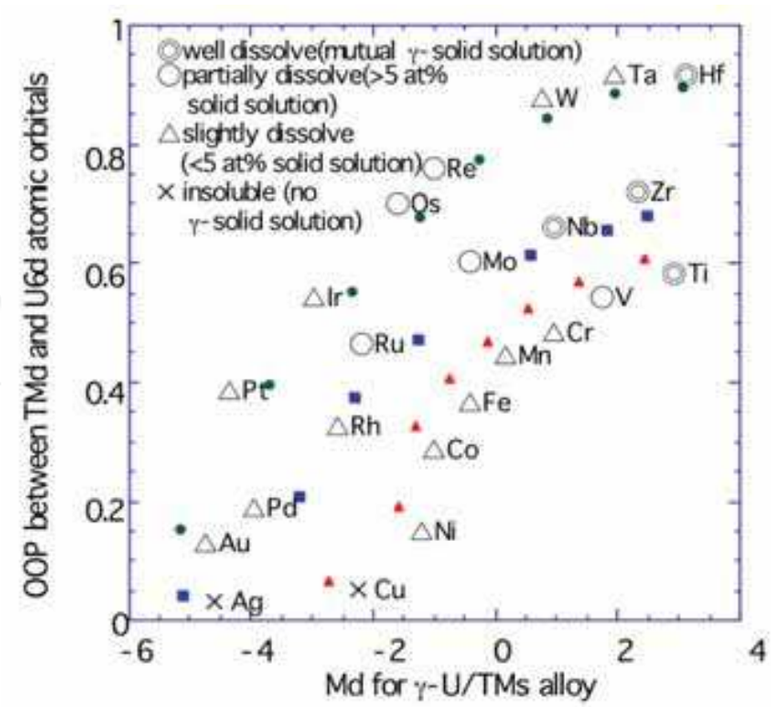

Fig. 16. OOP-Md plot of γ–U/ TM alloys [Kurihara et al., (2011)]

lower left hand on the map, whereas those with a higher MSS in an upper right hand. Consequently, the OOP–Md map could be useful for designing γ-U/ TM alloys. We believe that the present findings can be used for not only the γ-U/ TM alloy system but also other actinide alloys used as nuclear fuels for advanced reactors.

6. Summary and perspective

We have performed R-DFT calculations for understanding and designing γ-U/ TM alloys as a typical example of nuclear fuels. Md and OOP have a good correlation with MSS of γ-U/ TM alloys, and become a more suitable parameter to determine the magnitude of MSS than metallic radius as previously proposed by Hume-Rothery. The present parameters, Md and OOP, demonstrated that a stronger covalent bonding between TMd and U atoms gives rise to a larger MSS of γ-U/ TM alloys, whereas a stronger ionic bonding between them gives rise to a smaller MSS.

In summary, the magnitude of MSS was successfully explained in terms of the stabilization energy (ΔE) caused by the U6d-TMd orbital interactions for γ-U/ TM alloys. In addition, the exponential dependence of MSS on Md and OOP was also interpreted by considering the equilibrium constant based on thermodynamics of the substitution model for γ-U/ TM alloys. The OOP-Md map was useful to determine the magnitude of MSS for γ-U/ TM alloys. Finally, the present approach could be applied to understand and design the other alloy systems used as nuclear fuels for advanced reactors.

7. Acknowledgments

The authors are great thankful to Dr. M. Hirata (Japan Atomic Energy Agency) for valuable and helpful comments on this article, and also thankful to Profs. H. Adachi and T. Mukoyama (Kyoto University), and Prof. R. Sekine (Shizuoka University) for fruitful discussion on uranium molecules such as UF_6. Finally, this review article is sincerely dedicated to late Prof. H. Nakamatsu (Kyoto University).

8. References

Adachi. H., et al., (1978). *J. Phys. Soc. Jpn.* Vol. 45, pp. 875-883.
Alonso. P. R., et al., (2009). *Phys.* Vol. B 404, pp. 2851-2853.
Bethe, H., (1929). *Ann. Phys.* Vol. 3, pp. 133-208.
Buzzard. R. W., (1955). Progress Report-*Alloying Theory*, NBS-4032.
Chernock. W. & Horton. K. E., et al., (1994). IAEA *TECDOC-791*, p. 68, Vienna.
Chiotti. P., et al., (1981). IAEA *STI/PUB/424/5*, Vienna.
Ejima, T., et al., (1993). *Physica B,* Vol. 186/ 188, pp 77-79.
Erode, P., et al., (1983). *The Physics of Actinides Compounds,* Plenum Press. New York.
Fuggle, A. F., et al., (1974). *J. Phys. F,* Vol. 4, pp 335-342.
Gelius, U., (1974). *J. Electron Spectrosc. Relat. Phenom.* Vol. 5, pp. 985-1057.
Hirata. M., et al., (1997). *J. Electron Spectrosc. Relat. Phenom.* Vol. 83, pp. 59-64.
Holden. A. M., (1958). *Physical Metallurgy of Uranium*, Addison-Wesley, New York.
Hückel . E., (1931). *Z. F. Phys.* Vol. 70, pp. 204-286.

Hume-Rothery. M. & Raynor. G. W., (1954). *Structure of Metals and Alloys,* Institute of Metals, London.
Kaufman. A. R., (1962). *Nuclear Reactor Fuel Elements*, Interscience/ Butterworth, USA.
Kim. K. –H., et al., (1999). *J. Nucl. Mater.* Vol. 270, pp. 315-321.
Kim. K. -H., et al., (2002). *Nucl. Eng. Design* Vol. 211, pp. 229-235.
Kurihara. M., et al., (1999). *J. Alloys Compd.* Vol. 283, pp. 128-132.
Kurihara. M., et al., (2000). *J. Nucl. Mater.* Vol. 281, pp. 140-145.
Kurihara. M., et al., (2004). *J. Nucl. Mater.* Vol. 326, pp. 75-79.
Kurihara. M., et al., (2008). *Prog. Nucl. Ener.* Vol. 50, pp. 549-555.
Kurihara. M., et al., (2011). *J. Alloys Compd.* Vol. 509, pp.1152-1156.
Landa. A., et al., (2009). *J. Alloys Compd*. Vol. 478, pp. 103-110.
Li. Z. S., et al., (2009). *J. Alloys Compd*. Vol. 476, pp. 193-198.
Meyer, J., et al., (1989). *Comput. Phys. Commum.* Vol. 54, pp. 55-73.
Meyer. M. K., et al., (2002). *J. Nucl. Mater.* Vol. 304, pp. 221-236.
Morinaga. M., et al., (1984). *J. Phys. Soc. Jpn.* Vol. 53, pp. 653-663.
Morinaga. M., et al., (1985a). *J. Phys. F, Met. Phys.* Vol. 15, pp. 1071-1084.
Morinaga. M., et al., (1985b). *Philos. Mag. A* Vol. 51, pp. 223-246.
Morinaga. M., et al., (1985c). *Philos. Mag. A* Vol. 51, pp. 247-252.
Morinaga. M., et al., (1991). *J. Phys.: Condens. Matter.* Vol. 3, pp. 6817-6827.
Morinaga. M., et al., (2005). *Alloy design based on the DV-Xα cluster method*. (Adachi, H et al., Eds.), Hartree-Fock-Slater Method for Material Science, The DV-Xα Method for Design and Characterization of Materials, Springer Series in Materials Science, Vol. 84, pp. 23-48, ISBN-10-3-540-24508-1, Springer, Berlin, Heidelberg, New York.
Mulliken. R. S., (1955a). *J. Chem. Phys.* Vol. 23, pp. 1833-1840.
Mulliken. R. S., (1955b). *J. Chem. Phys.* Vol. 23, pp. 1841-1845.
Mulliken. R. S., (1955d). *J. Chem. Phys.* Vol. 23, pp. 2343-2347.
Mulliken. R. S.,(1955c). *J. Chem. Phys.* Vol. 23, pp. 2338-2342.
Ogawa. T., et al., (1955). *J. Nucl. Mater.* Vol. 223, pp. 67-71.
Onoe. J., et al., (1992). *J. Electron Spectrosc. Relat. Phenom*. Vol. 60, pp. 29-36.
Onoe. J., et al., (1993). *J. Chem. Phys.* Vol. 99, pp. 6810-6817.
Onoe. J., et al., (1994). *J. Electron Spectrosc. Relat. Phenom.* Vol. 70, pp. 89-93.
Park. J. J. & Buzzard. R. W., (1957). *TID-7526 (Pt. 1)* pp. 69-102.
Pauling L., (1960). *The Nature of the Chemical Bond*, third ed. Cornell Univ. Press, New York.
Rosen. A & Ellis. D. E., et al., (1975). *J. Chem. Phys.* Vol. 62, pp. 3039-3049.
Rosen. A., et al., (1976). *J. Chem. Phys.* Vol. 65, pp. 3629-3634.
Schadler, G.H., (1990). *Solid State Commum.* Vol. 74, pp. 1229-1231.
Scofield, J. H., (1976). *J. Electron Spectrosc. Relat. Phenom.* Vol. 8, pp. 129-137.
Sedmidudbsky. D., et al., (2010). *J. Nucl. Mater.* Vol. 397, pp. 1-7.
Yamagami, H. & Hasegawa, A. (1990). *J. Phys. Soc. Jpn.* Vol. 59, pp. 2426-2442.
Zachariasen W. H., (1973). *J. Inorg. Nucl. Chem.* Vol. 35, pp. 3487-3497.

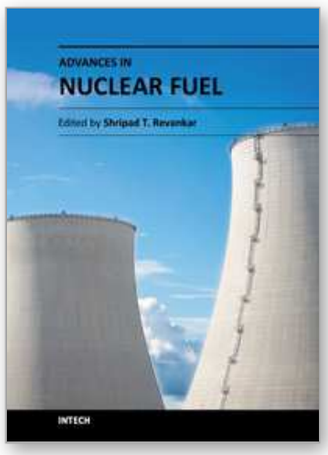

Advances in Nuclear Fuel

Edited by Dr. Shripad T. Revankar

ISBN 978-953-51-0042-3
Hard cover, 174 pages
Publisher InTech
Published online 22, February, 2012
Published in print edition February, 2012

Worldwide there are more than 430 nuclear power plants operating and more plants are being constructed or planned for construction. For nuclear power to be sustainable the nuclear fuel must be sustainable and there should be adequate nuclear fuel waste management program. Continuous technological advances will lead towards sustainable nuclear fuel through closed fuel cycles and advance fuel development. This focuses on challenges and issues that need to be addressed for better performance and safety of nuclear fuel in nuclear plants. These focused areas are on development of high conductivity new fuels, radiation induced corrosion, fuel behavior during abnormal events in reactor, and decontamination of radioactive material.

InTech Europe
University Campus STeP Ri
Slavka Krautzeka 83/A
51000 Rijeka, Croatia
Phone: +385 (51) 770 447
Fax: +385 (51) 686 166
www.intechopen.com

InTech China
Unit 405, Office Block, Hotel Equatorial Shanghai
No.65, Yan An Road (West), Shanghai, 200040, China
中国上海市延安西路65号上海国际贵都大饭店办公楼405单元
Phone: +86-21-62489820
Fax: +86-21-62489821

IntechOpen